Electronic Supplementary Material (ESI) for Nanoscale.

Supporting Information

Magnetic Enrichment of Immuno-Specific Extracellular Vesicles for Mass Spectrometry Using Biofilm-Derived Iron Oxide Nanowires

Quang Nghia Pham,[a] Marnie Winter,*[a] Valentina Milanova,[a] Clifford Young,[b] Mark R. Condina,[a] Peter Hoffmann,[b] Nguyen T. H. Pham,[c] Tran Thanh Tung,[d] Dusan Losic,[d] Benjamin Thierry*[a]

[a]Future Industries Institute, University of South Australia, Mawson Lakes Campus, Mawson Lakes, Adelaide, South Australia 5095, Australia

[b]Clinical and Health Science, University of South Australia, 5000, Australia

[c]Key Centre for Polymers and Colloids, School of Chemistry, The University of Sydney, Sydney, New South Wales 2006, Australia

[d]School of Chemical Engineering and Advanced Materials, The University of Adelaide, Adelaide, South Australia 5005, Australia

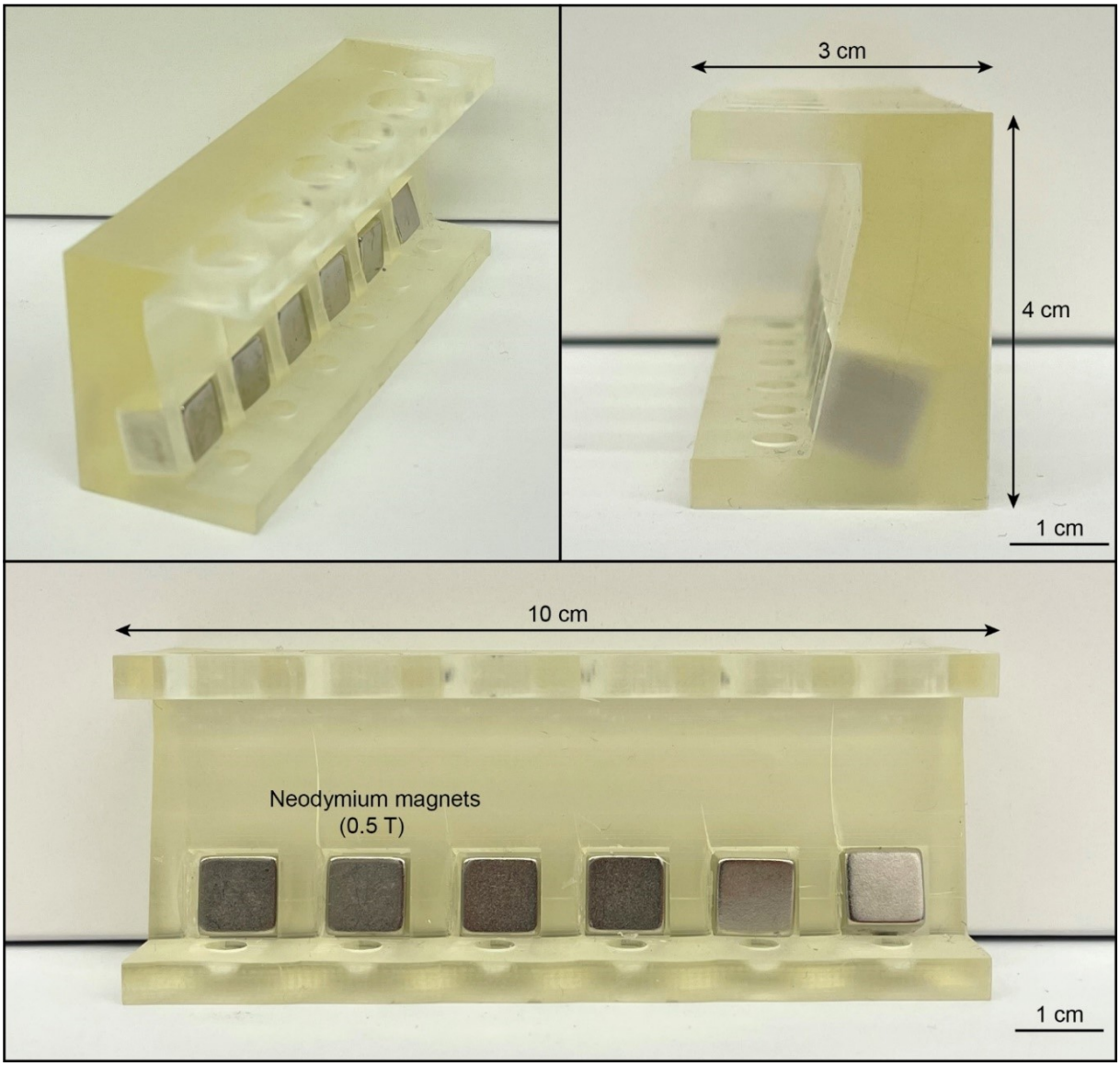

Fig. S1 Images of the in-house 3D-printed magnetic separation rack used for immuno-magnetic isolation of EVs. The rack was designed to fit 1.5-mL and 2.0-mL Eppendorf tubes and neodymium magnets (Grade N42, 0.5 T, 10 × 10 × 10 mm).

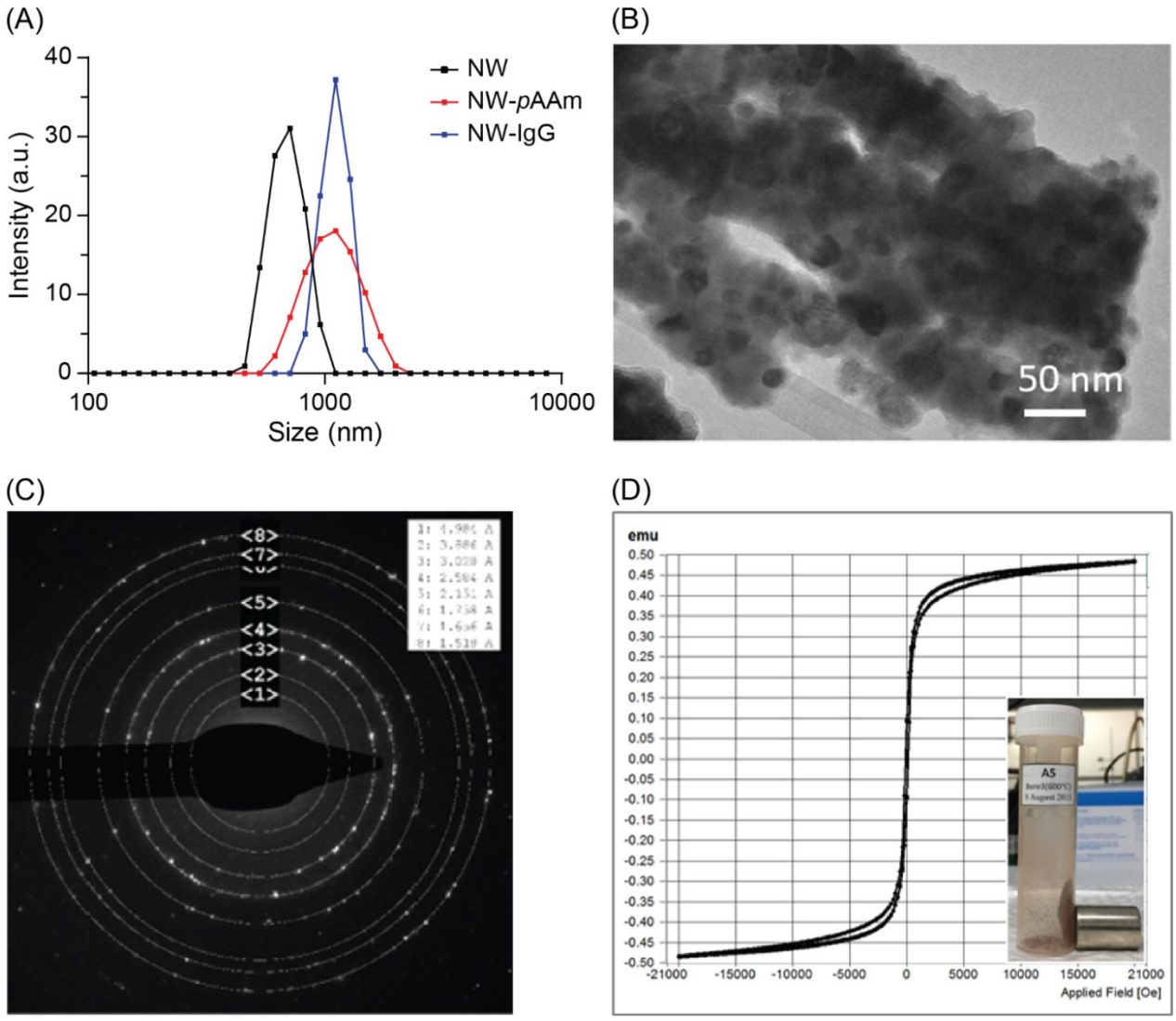

Fig. S2 (A) Monitoring of changes in NWs' scattering by dynamic light scattering during the coating procedure. (B) Transmission electron microscope image and (C) diffraction pattern of iron oxide NWs showing wire-like structures with diameters of 50–80 nm and polycrystalline rings with lattice refractions corresponding to a mixture of magnetite and hematite structures. (D) The magnetic hysteresis curves of iron oxide NWs revealing a ferromagnetic behaviour of the material with a photo (inset) demonstrating the magnetic property of iron oxide NWs using a magnet.

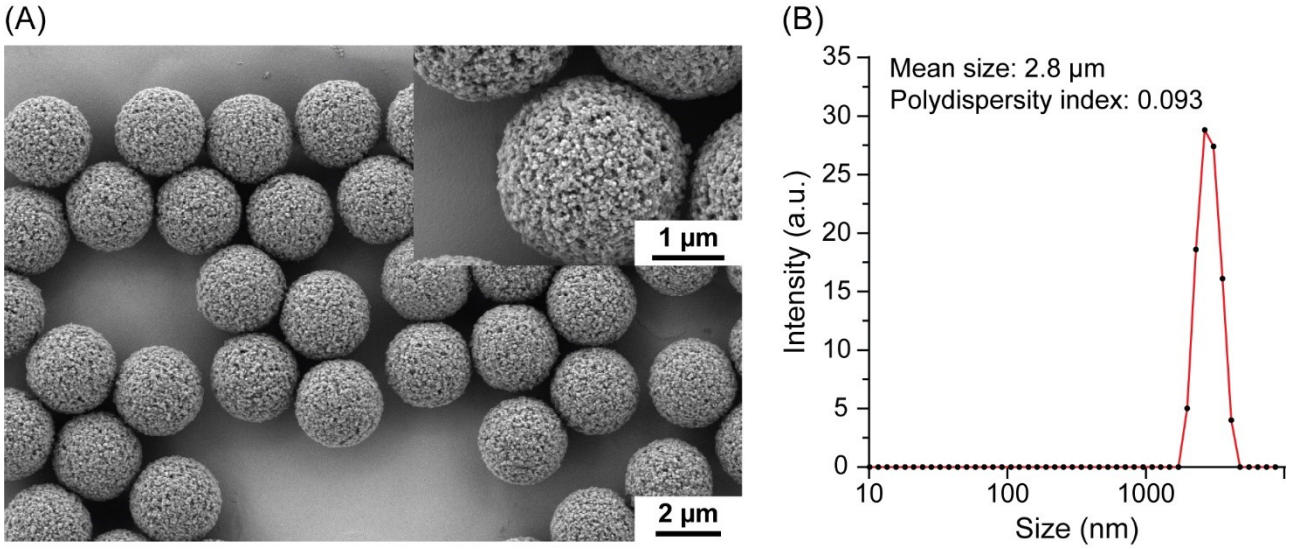

Fig. S3 (A) Scanning electron microscopy images of Dynabeads M-270 carboxylic acid. Inset is the SEM image at a higher magnification. (B) Dynamic light scattering size measurement of Dynabeads.

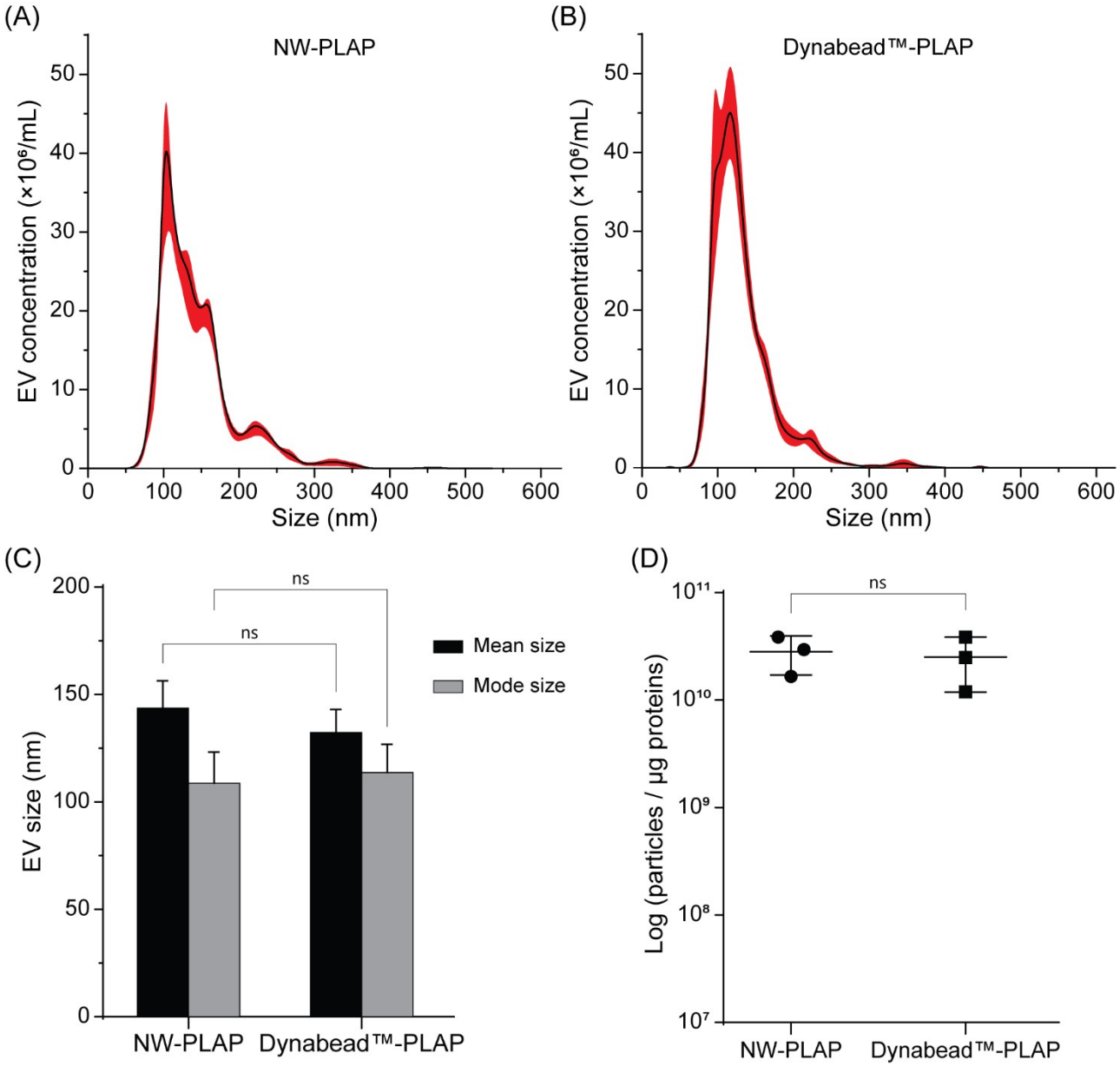

Fig. S4 Nanoparticle tracking analysis of eluted EVs enriched by (A) NW-PLAP and (B) Dynabead™-PLAP. (C) Mean size and mode size of eluted EVs. (D) The particle to protein ratio of PLAP+ve EVs enriched by NW-PLAP and Dynabead™-PLAP. Data are presented as means + SD (n = 3, independent Student's t-test with 95% confidence interval, ns = not significant, $p > 0.05$).

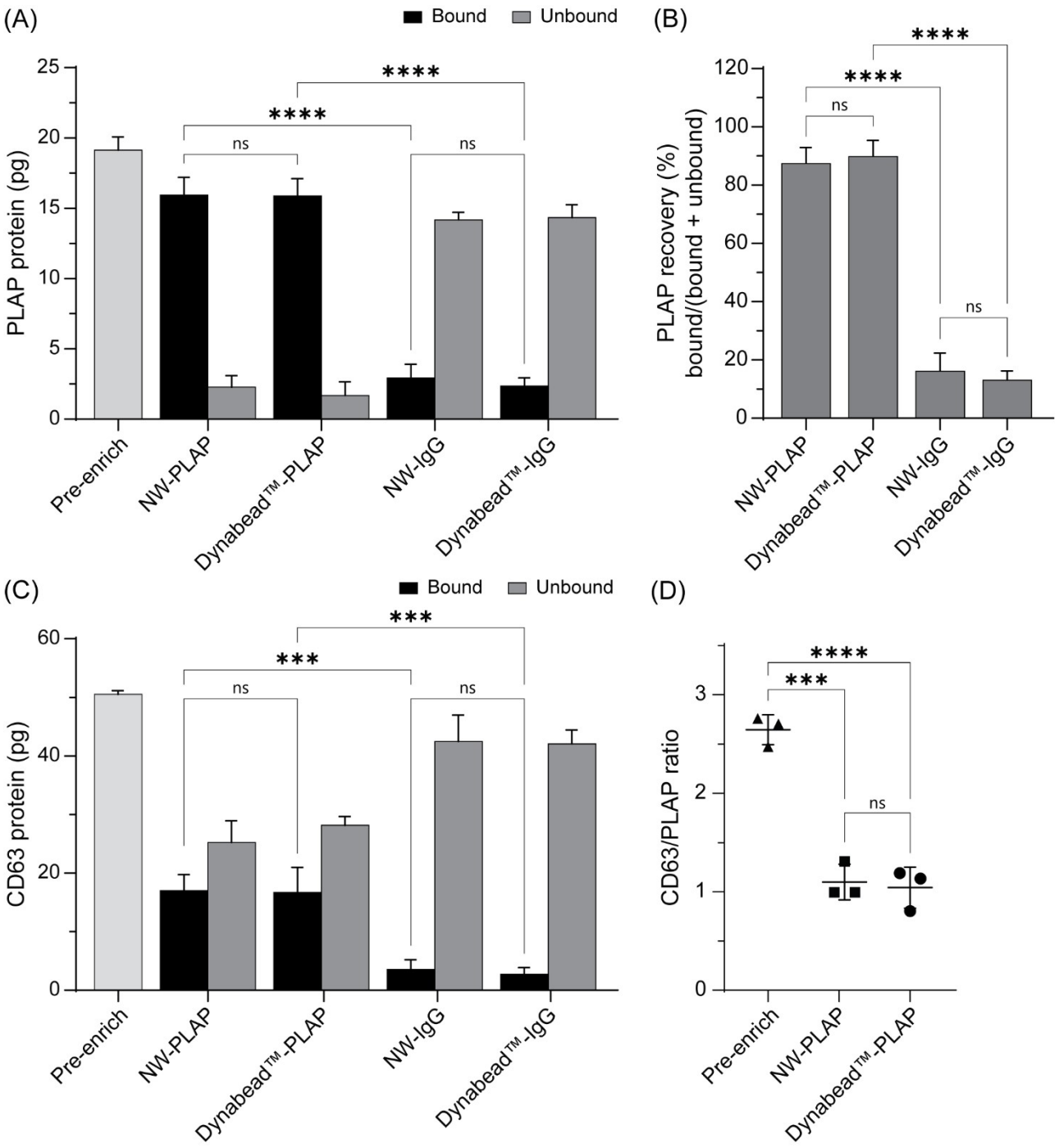

Fig. S5 (A) Quantification of PLAP in the pre-enriched sample (after ultracentrifugation of BeWo cell culture media), EVs captured by NWs and Dynabeads conjugated with either anti-PLAP or irrelevant IgG (bound) and the corresponding supernatants (unbound). (B) PLAP recovery of EVs enriched by NW-PLAP and Dynabead™-PLAP presented by the ratio of bound to the total of bound and unbound. (A) Quantification of CD63 in the pre-enriched sample, bound and unbound of NW-PLAP and Dynabead™-PLAP. (D) The ratio of CD63 to PLAP (pg/pg) calculated for the pre-enriched sample, NW-PLAP and Dynabead™-PLAP. Data are presented as means + SD (n = 3, one-way ANOVA with Tukey's post-test, ns = not significant, ***$p < 0.001$, and ****$p < 0.0001$).

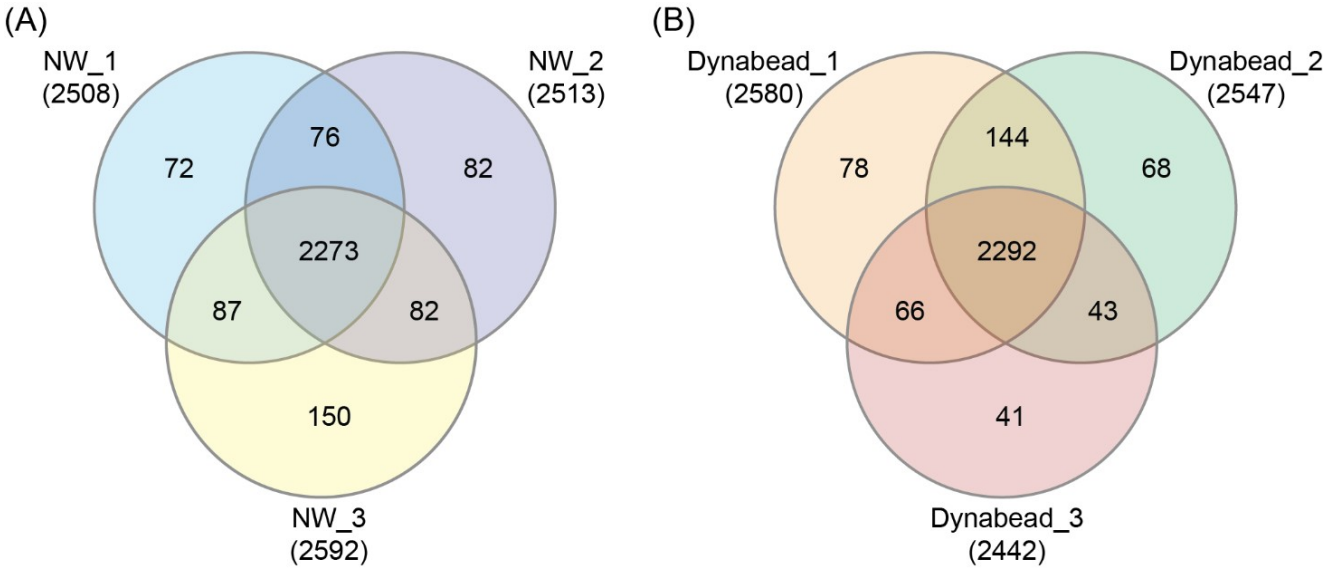

Fig. S6 Overlap of protein groups enriched by three replicates of (A) NW-PLAP and (B) Dynabead™-PLAP.

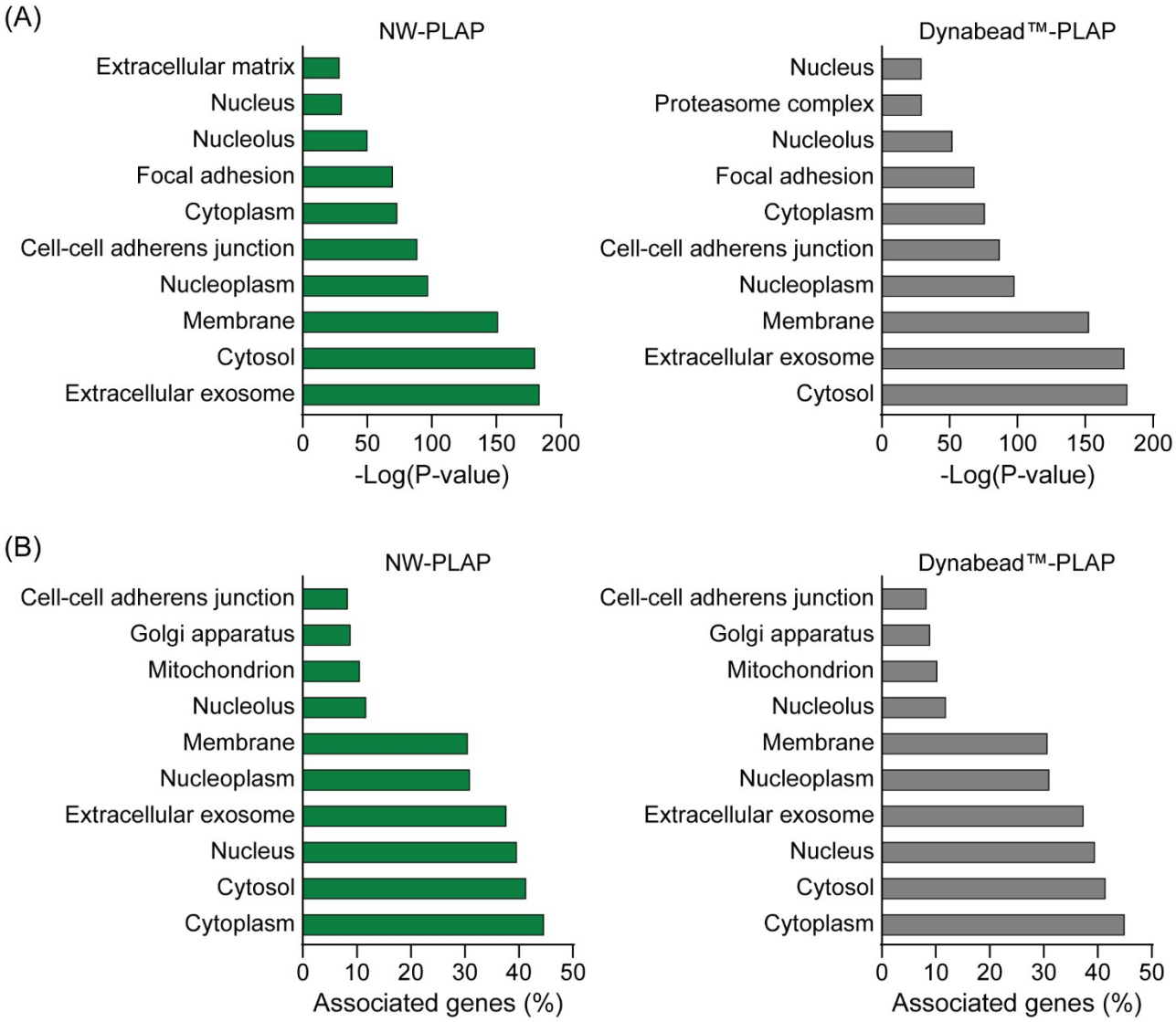

Fig. S7 Gene ontology (GO) analyses of the protein groups in BeWo EVs enriched by NW-PLAP and Dynabead™-PLAP according to DAVID Bioinformatics Resources. Top 10 GO categories were reported for (A) Cellular component and (B) The percentage of associated genes.

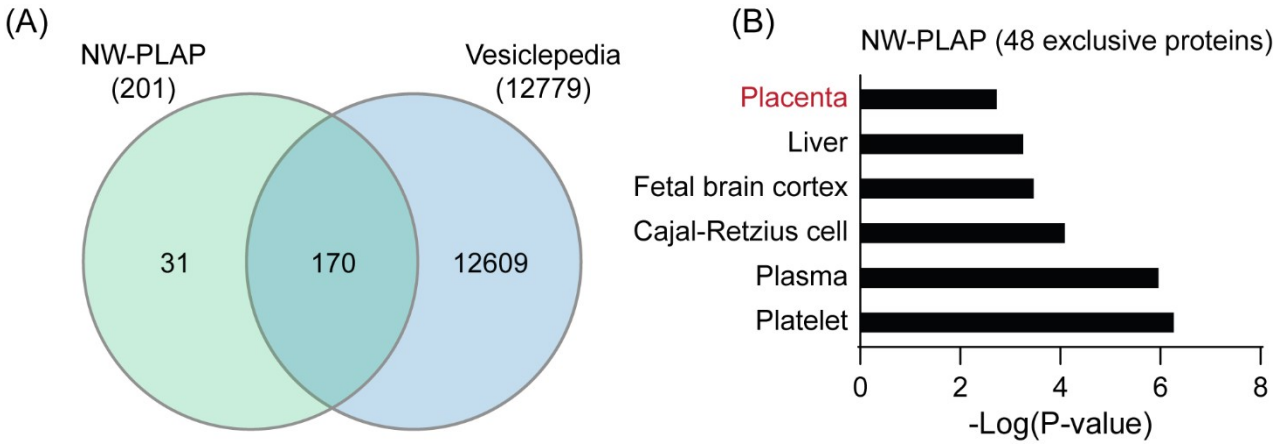

Fig. S8 (A) Venn diagrams showing overlapping proteins of plasma-derived EVs enriched using NW-PLAP from a 100 µL biobanked plasma sample of a preeclamptic pregnancy. (B) Tissue expression of identified proteins analysed by DAVID Bioinformatics Resources. Top 6 categories are reported and ranked by P-value for NW-PLAP.

Table S1 Batch-to-batch validation of antibody conjugation to NWs

NW samples	XPS elemental composition (%)		
	C	N	O
NW Batch 1 Antibody conjugation 1	47.79	8.13	44.09
NW Batch 1 Antibody conjugation 2	45.80	7.51	46.69
NW Batch 2 Antibody conjugation 1	49.12	7.85	43.03